RSC Advances




ROYAL SOCIETY OF CHEMISTRY

www.rsc.org/advances

# Internal friction characteristic and analysis of in-plane natural frequency of trilayer complexes formed from graphenes and boron nitride nanosheets

Jianhui Yuan[a,b] and K. M. Liew[*,b,c]

[a]*School of Physics and Electronic Science, Changsha University of Science and technology, Changsha 410114, China*

[b]*Department of Architecture and Civil Engineering, City University of Hong Kong, Kowloon, Hong Kong SAR*

[c]*City University of Hong Kong Shenzhen Research Institute Building, Shenzhen Hi-Tech Industrial Park, Nanshan District, Shenzhen, China*

## Abstract

The internal friction and in-plane natural frequency of a trilayer complex formed by a monolayer graphene sandwiched in bilayer boron nitride nanosheets (BN/G/BN) and graphenes (G/G/G) are studied by using molecular dynamics. The investigation shows that the internal friction coefficients for BN/G/BN (~0.025) are significantly higher than those of G/G/G (~0.015). The coefficients for both G/G/G and BN/G/BN increased with external pressure. The speed of increase is divided into quick increase, slow increase and saturation stage. The internal friction coefficients for G/G/G and BN/G/BN follow the simple microscopic theory of Amontons's laws only when the external pressure exceeds 170nN. These findings are expected to help enhance understanding of the mechanism of nano-tribology and provide an effective micro-control method of internal friction. Subsequent analysis shows that the

[*] Corresponding author. Tel.: +852 3442 7601. E-mail address: kmliew@cityu.edu.hk (K.M. Liew).

in-plane natural frequency of mid-layer graphene in BN/G/BN is significantly higher than in G/G/G and both increase as the external pressure grows. Moreover, the natural frequency of mid-layer graphene in trilayer complexes, especially in BN/G/BN, is extremely sensitive to external pressure loads.

**Keywords:** trilayer nanosheets; molecular dynamics; internal friction; natural frequency; pressure loads

## 1. Introduction

The graphite, with a layered structure, is widely used in lubricated systems because the weak interaction between layers leads to low friction and wear during relative sliding. It is one of the very important solid lubricants. Graphite and molybdenum disulfide are typical low friction materials while mica is not [1]. These materials are used as solid lubricants in an artificial satellite in which liquid lubricants, such as hydrocarbons, are not used because of the high vacuum environment. Some additives are mixed into automotive lubricants in order to generate a solid lubricant film in the sliding contact area due to the heat and shear, which often undergo tribochemical reactions. Graphene, which consists of a single or several layers of graphite, has attracted broad interest because of its unique electronic, thermal and mechanical properties [2-5] and may prove to be an important material for electronics and micro- or nano-electromechanical systems (M/NEMS) in the future [6-9]. Should graphene become a material of interest for M/NEMS, its interfacial and mechanical properties will play an important role in determining the overall system performance. As a

model material, an in-depth investigation leading to an improved understanding of mechanical and interfacial behavior of graphene would advance knowledge of the mechanistic origins of friction and potentially lead to its application in future M/NEMS devices.

Friction is one of the most familiar physical phenomena and has been investigated since long due to its importance in various kinds of machinery and in many systems in science. In the last two decades atomic scale friction has attracted much attention for gaining understanding of fundamental mechanisms of macroscopic friction and in many fields related to high precision engineering such as nanomachines [10]. In application process of graphene, the frictional behavior will be a big factor that affects its performance. Therefore, the research on friction characteristics of graphene has considerable practical significance. However, for a long time, people's understanding of friction has been very limited as it has been limited to macro level and little is known about the microscopic mechanism of macroscopic friction. To understand the mechanisms underlying its friction behavior, people's understanding of friction has gradually gone deeper into molecular, atomic levels until tools such as atomic force microscope (AFM) [11] and friction force microscope (FFM)[12] become available. Since the AFM and FFM studies cannot provide direct evidence of what is happening in the interface buried between the probe and the graphene, molecular dynamics (MD) simulations have been introduced to help explain the observed behaviors. As a result, a new academic subject nano-tribology has come into existence. For now, FFM and AFM have been

successfully applied for investigation of frictional surfaces of diamond and graphite, and provide an objective and direct image for people to understand the friction at atomic scale [13, 14, 15]. Along with the deepening of the experiments on the understanding of the friction, theoretical research on nano-tribology has made great progress; the harmonic oscillator model of nano-tribology has been popularly approved [16]. Based on the concept of the harmonic oscillator model, by using MD and the approximate method where the relaxation energies between the harmonic oscillators are equal to the potential barriers between the maximum and minimum potential energy in the process of interfacial sliding, the friction on the atomic scale has been investigated in literature [17, 18]. The results are in good agreement with the experiment. Matsushita et al. [19] and Zaidi et al. [20] investigated atomic scale friction between clean graphite surfaces and behavior of graphite in friction under various environments by using MD. Neitola et al. [21] investigated the nanoscale friction between two graphite layers placed in contact by using ab initio methods. Recent measurements have revealed a novel trend where the frictional resistance to sliding is smaller on bilayer graphene than on single layer graphene [22, 23]. This trend has been confirmed through another set of experiments that included up to four layers of graphene and other layered materials [4, 24, 25]. The latter experimental measurements are explained by a puckering effect where a wrinkle in front of the FFM tip that resists sliding is more dominant with fewer layers.

In the research on vibration properties, Murmu and Pradhan [26] employed the nonlocal elasticity theory for analysis of vibration of rectangular single layered

graphene sheets (SLGS) embedded in an elastic medium. They have used both Winkler-type and Pasternak-type models for simulating the interaction of graphene sheets with a surrounding elastic medium. They reported that the natural frequencies of SLGS are strongly dependent on the small scale coefficients. Pradhan and Phadikar [27] investigated vibration of embedded multilayered graphene sheets (MLGSs) based on the nonlocal elasticity theory. They showed that the small scale effect is quite important and needs to be included in the continuum model of graphene sheet. Murmu and Pradhan [28] studied the free in-plane vibration of nanoplates by nonlocal continuum model and obtained explicit relations of natural frequencies through direct separation of variables. Specifically, graphene has recently been extensively taken into account for designing nanoresonators that can exhibit high-frequency dynamic range [29, 30] with favorable high Q factors [31, 32]. The high-frequency dynamics of graphene is attributed to its excellent mechanical properties such as Young's modulus of approximately 1 TPa [33, 34]; it is noted that a resonant frequency is linearly proportional to the square root of Young 's modulus when a device operates in harmonic oscillation [35, 36]. Until recently, most research works [30, 31, 37] have focused on harmonic oscillation of a graphene resonator.

Many theoretical and experimental studies on mono- or bi-layer graphenes and boron nitride nanosheets (BNNSs) have examined structures of nanosheets and some of the conclusions have been useful in engineering applications [38-40]. However, the study on their trilayer systems still seems very insufficient. Because of their possible applications in nano-electronic devices, it has also been the subject of several recent

studies. The trilayer graphene system exhibits stacking-dependent electronic properties under the influence of a perpendicular electric field, with the semiconducting ABC stacked trilayer showing a large tunable gap relative to the metallic ABA stacked trilayer [41, 42]. While monolayer graphene retains its gapless feature in the presence of a perpendicular electric field, a BN/graphene/BN trilayer system shows stacking-dependent energy gap tunability [43, 44]. However, internal friction and in-plane vibration properties of the trilayer graphene and BN/graphene/BN systems do not appear to have been covered in extant research.

To take full advantage of the structural performance of multilayer architecture in any environment, we have studied structural stability and elastic properties of monolayer and bilayer carbon nanotube, graphene and BN nanotubes (nanosheet) by using MD simulation [45-49]. In this study, we further investigate the trilayer architecture based on these studies. This paper mainly studies the hybrid trilayer system monolayer graphene inserted into bilayer graphene and BNNSs (G/G/G and BN/G/BN). Their interlaminar interaction, internal friction and interlayer in-plane natural frequency in trilayer G/G/G and BN/G/BN nanosheets are investigated by calculating and analysing their system energies and electron density after deformation under different conditions. The differences between G/G/G and BN/G/BN are compared and some useful observations and conclusions are obtained. These results can provide some important information for the proper utilization of trilayer nanosheets under various practical conditions.

## 2. Computational model and method

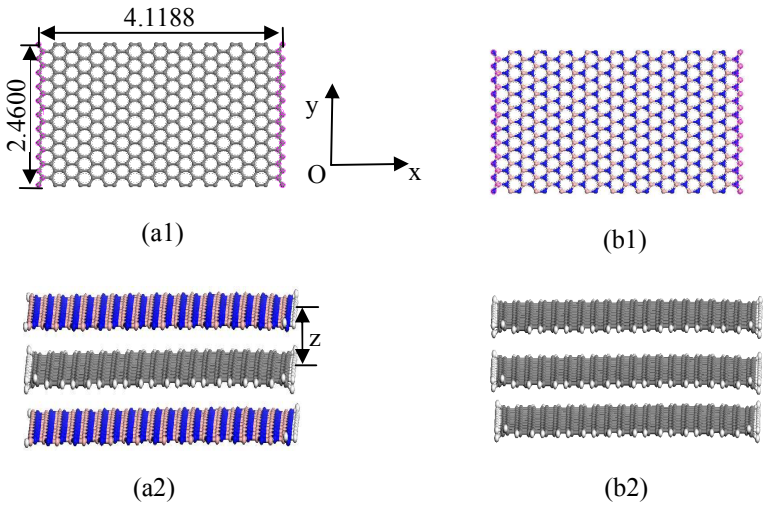


Fig. 1. Geometric models of trilayer BN/G/BN and G/G/G (unit: nm).

The structural model for graphenes and BNNSs was set up according to atomic space coordinates. The nanosheets in this study can be achieved using 20 and 10 repeat basic units in length and width. The corresponding sizes were 4.1188 and 2.4600 nm, as shown in Figs. (1)a1 and (1)b1, respectively. The trilayer BN/G/BN and G/G/G complex nanosheets were constructed through the parallel setting of a monolayer graphene sandwiched between bilayer BNNSs and graphenes with different interlayer distances. Dangling bonds existed at the atoms around the borders of the nanosheets, which were considered more active. Some hydrogen atoms were used as an auto-update link of the boundary of the nanosheets to achieve electron saturation, as shown in Figs. (1)a2 and (1)b2. The original structure optimization, system energies and deformation electron density were calculated and analyzed using the universal force field (UFF)[50] and the density functional theory (DFT) method.

The UFF, a molecular mechanics force field, is where the force field parameters are estimated using general rules based only on the element, its hybridization and its

connectivity. The potential energy of the UFF is expressed as the sum of bonded and non-bonded interactions:

$$E_{@} = E_R + E_\theta + E_\tau + E_\omega + E_v + E_{el} \ . \quad (1)$$

The bonded interactions include bond stretching $E_b$, the angle bending $E_\theta$, the dihedral angle torsion $E_\tau$ and the inversion terms $E_\omega$, whereas non-bonded interactions include the van der Waals interaction $E_v$ and the electrostatic interaction $E_{el}$. The UFF includes a parameter generator that calculates force field parameters by combining atomic parameters. Thus, force field parameters for any combination of force field types can be generated as required. For further details, including the generator equations, see the literature [50-52].

## 3. Results and discussion

### 3.1 Interlaminar interaction among trilayer nanosheets

This article mainly describes the friction forces caused by the electron interaction between atomic layers, regardless of the phonons interactions. The interaction energy is applied to the interaction among nanosheets, and its calculation method is as follows:

$$E_i = E_{@} - \sum_n E_n = \begin{cases} E_{@} - (E_G + 2E'_G) & for \quad G/G/G \\ E_{@} - (E_G + 2E_{BN}) & for \quad BN/G/BN \end{cases} \quad (2)$$

In the formula, $E_i$ represents the interaction energy, $E_{@}$ represents the total energy of the system, $E_n$ represents the single point energy of each layer of the nanosheet, $\sum_n$ represents the sum of the single point energy of all nanosheets in the trilayer system. The results of computer simulation for single-point energies of

graphene and BNNS in BN/G/BN and G/G/G are shown in table 1. The interlayer distances for trilayer nanosheets are reduced gradually from 0.347 to 0.317nm for BN/G/BN and 0.341 to 0.311nm for G/G/G along the direction of surface normal in steps of 0.05Å. The interaction energies at each step length are calculated during the procedure of the still compression (Fig. 2).

Table 1. Single-point energies of graphene and BNNS in BN/G/BN and G/G/G ($10^6$ J/mol)

| complex | BN/G/BN | | G/G/G | |
|---|---|---|---|---|
| location | Up (down) layer | Mid-layer | Up (down) layer | Mid-layer |
| $E_n$ | 5.20149 | 7.26364 | 7.26019 | 7.26178 |
| $E_{nv}$ | 4.24088 | 5.84545 | 5.80947 | 5.85349 |

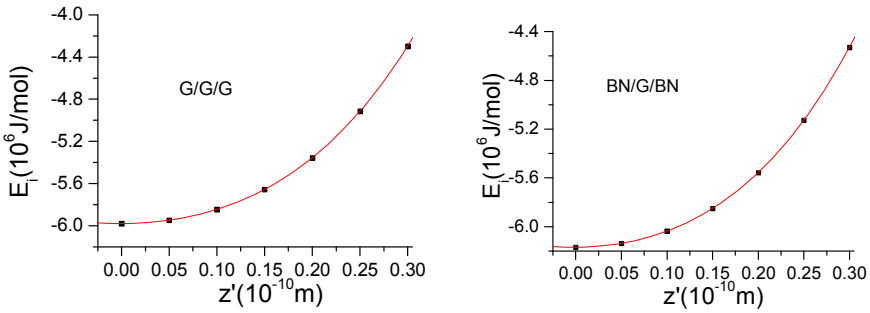


Fig. 2. The interaction energies as a function of length of compression in G/G/G and BN/G/BN.

The normal pressure ($F_N$) at different interlayer distances can be obtained according to the differential operation of interaction energy ($E_i$) with respect to interlayer distances (z):

$$F_N = -\partial E_i(z)/\partial z = \partial E_i(z')/\partial z' \quad (3)$$

where $z'$ represents the length of compression. By Fig. 2, the normal pressures at different locations of compression for G/G/G and BN/G/BN can be calculated. The results are shown in table 2 and Fig. 3. It can be seen that compressing BN/G/BN are a bit easier than G/G/G, suggesting that the interlaminar repulsion interactions in BN/G/BN are a little less than in G/G/G.

Table 2. The normal pressures at different lengths of compression (nN)

| $z'$ (Å) | 0.05 | 0.1 | 0.15 | 0.2 | 0.25 | 0.3 |
|---|---|---|---|---|---|---|
| G/G/G | 21.25271 | 47.20411 | 80.06473 | 121.5035 | 173.6097 | 238.9905 |
| BN/G/BN | 20.9615 | 46.36965 | 78.33133 | 118.3702 | 168.375 | 230.6791 |

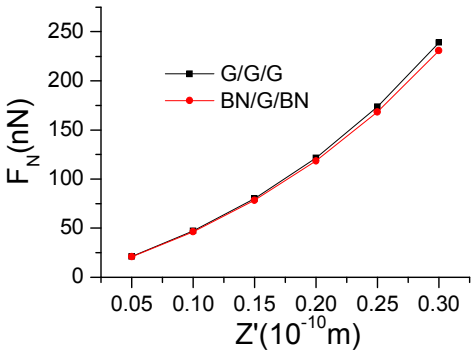


Fig. 3. The normal pressures as a function of length of compression in G/G/G and BN/G/BN.

## 3.2 Friction phenomenon among trilayer nanosheets

To examine the internal friction in the trilayer nanosheets, the mid-layer graphenes in G/G/G and BN/G/BN are applied to slide along the x direction in its plane. The loading scheme is as follows. At different lengths of compression along the normal direction of surface from 0.05 Å to 0.30 Å in steps of 0.05Å, the slide distances are designed from 0 to 0.4 nm for G/G/G and 0 to 0.46 nm for BN/G/BN at an incremental displacement step of 0.2 Å. The interaction energies at each step length are calculated during the procedure of the sliding. In addition, the periodical boundary conditions are applied to x and y directions so as to avoid the potential energy at different positions along the sliding path that exhibits a global gradually increasing trend when the sliding distance becomes larger, which is due to the increase of surface energy, while the periodic variation due to periodically changing neighboring atomic distances between layers can still be preserved. As a result, this concludes that the periodic variation of the sliding distance cannot be too large. According to the method described in [17], the potential energy at different positions along the sliding path can be calculated from the following formula:

$$U_{(x,F_N)} = E_i(x, z(x, F_N)) + A_{F_N}(x) - U_{\min}(x, F_N) \quad (4)$$

In the formula, $E_i(x, z(x, F_N))$ represents the interaction energy under a certain normal pressure at different position along the sliding path, $A_{F_N}(x)$ represents the work done by the normal pressure which compresses up-down layer nanosheets in trilayer nanosheets to different positions，and the last term $U_{\min}(x, F_N)$ represents the minimum potential energy over the entire sliding path and it is subtracted in the

formula so as to get the relative value of the potential energy. Formula (4) indicates that the potential energy at a position along the sliding path is only relevant to the position and the normal pressure. Fig. 4(A) shows the potential energies as a function of the sliding distances under different normal pressures in G/G/G and BN/G/BN. For convenience sake, representation of normal pressure in Fig. 4(A) is equivalently marked by the compression of the interlayer distances.

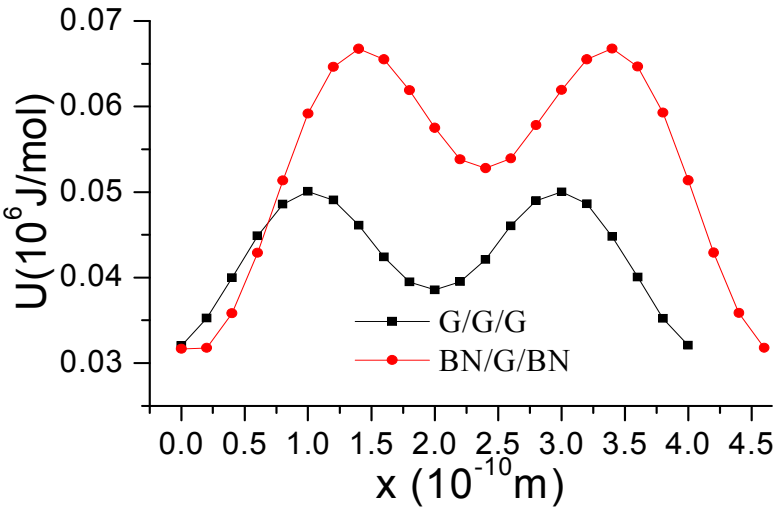


(A) Periodogram $z'$=0.05 Å

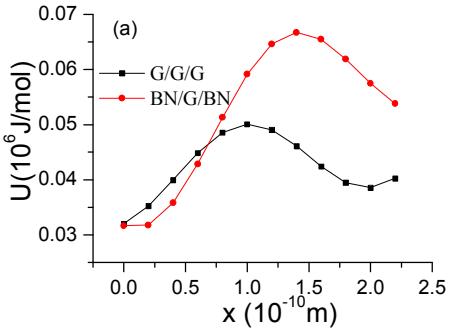


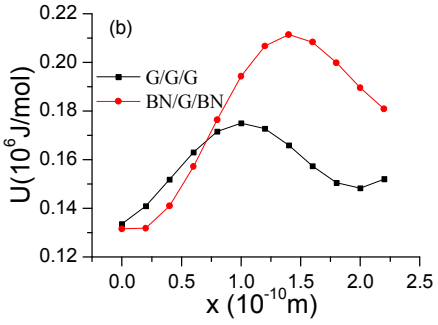

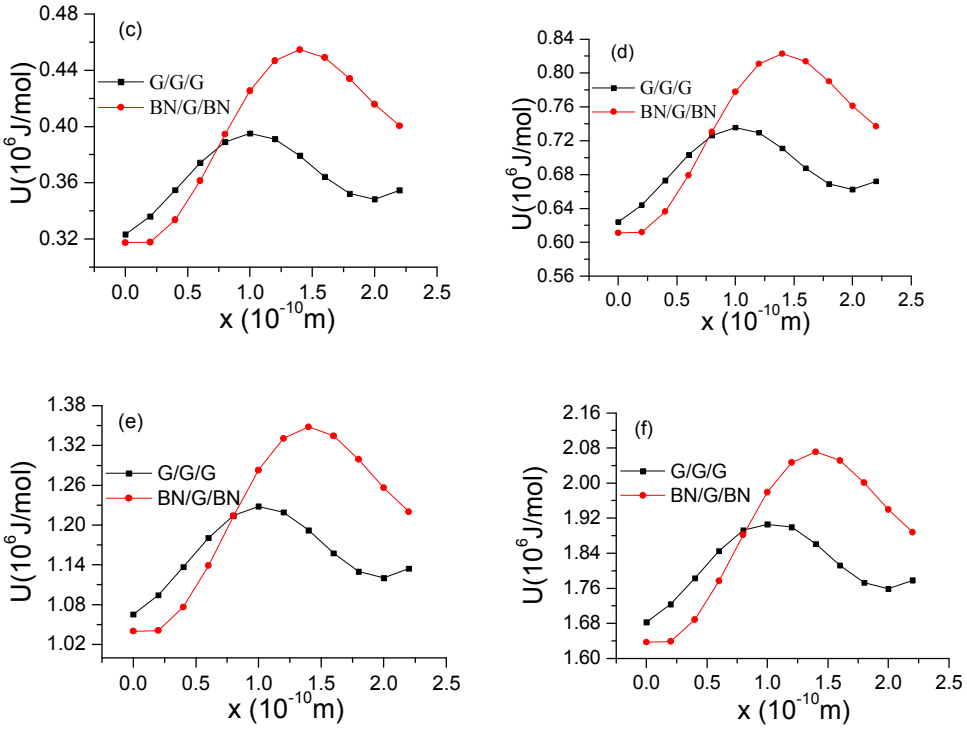


(B) Calculation diagrams

(a) $z'$=0.05 Å (b) $z'$=0.10 Å (c) $z'$=0.15 Å (d) $z'$=0.20 Å (e) $z'$=0.25 Å (f) $z'$=0.30 Å

Fig. 4. The potential energies as a function of the sliding distances under different normal pressures in G/G/G and BN/G/BN. (A) periodogram (B) calculation diagrams.

As shown in Fig. 4(A), the potential energies exhibit periodic variations with the sliding distance of mid-layer graphenes along x direction. This is because the neighboring atomic distances at all levels between mid-layer graphene and up-down layer nanosheets change periodically with the sliding. From Fig. 4(A), it is easy to see that the potential energies at all sliding distances increase uniformly with the

increase of the normal pressure, but the law of periodic changing of the potential energies with sliding distance remains almost unchanged. This is because the neighboring atomic distances at all levels between mid-layer graphene and up-down layer nanosheets decrease uniformly with the normal pressure, the potential repulsion between atoms increases and the system energy increases uniformly as pressure. But the distance between neighbouring atoms at all levels between mid-layer graphene and up-down layer nanosheets have the same trends under different magnitudes of pressure with the sliding of mid-layer graphene. To know the effect of frictional coefficients in different pressure, the potential energies for the length of compression as a function of the sliding distances are calculated, as shown in Fig. 4(B). The calculated curves are basically similar to that of Fig. 4(A). For the sake of simplicity, x larger than 2.2 Å is not shown in Fig. 4(B). In the process of the relative sliding, the system has to surmount the potential barriers between the interfaces. Based on the harmonic oscillator model, the numerical potential barrier equals to the work done by overcoming the friction. The friction force can be determined by the following formula:

$$f(x, F_N) = \partial U(x, F_N) / \partial x \tag{5}$$

where $f(x, F_N)$ is the friction force at a certain position and normal pressure along the sliding path. Under the normal pressure, the maximum potential barrier on the whole sliding path is as follows:

$$\Delta U_{\max}(F_N) = U_{\max}(F_N) - U_{\min}(F_N) \tag{6}$$

In the formula, $U_{\max}(F_N)$ and $U_{\min}(F_N)$ are the maximum and minimum

potential energies on the sliding path, respectively. Therefore, $\Delta U_{\max}(F_N)$ is the potential barrier for the mid-layer to surmount when the relative sliding occurs between up-down layers. The energy dissipated in friction along sliding path ($\Delta U_{\max}$) can also be related to the average friction force along the trajectory as [17]:

$$\Delta U_{\max} = \Delta A_f = \overline{f} \cdot \Delta x \tag{7}$$

where $\Delta A_f$ represents the work done against the friction forces, $\overline{f}$ is average force of friction, $\Delta x$ is the distance between maximum and minimum potential energy positions on the sliding path. Finally, an average coefficient of friction under the normal pressure is obtained by the average force of friction:

$$\mu = \frac{\overline{f}}{F_N} = \frac{\Delta U_{\max}}{F_N \cdot \Delta x} \tag{8}$$

According to the formula, when the mid-layer graphenes in G/G/G and BN/G/BN slide along the x direction in the plane, the internal friction coefficients under different pressures are calculated, as shown in Fig. 5.

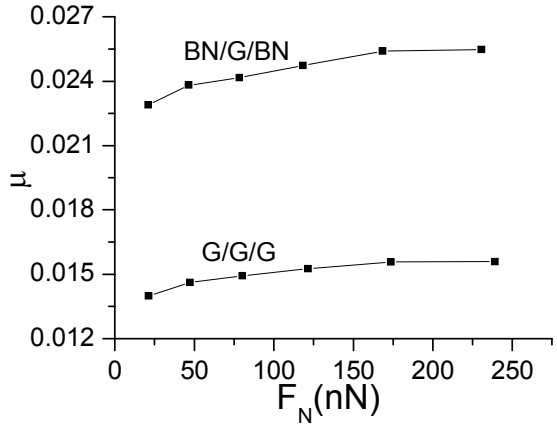


Fig. 5. The frictional coefficients as a function of different pressures.

Figure 5 shows that the internal friction coefficients for G/G/G are from 0.014 to 0.0156, and for BN/G/BN they are from 0.023 to 0.0255. The coefficients for BN/G/BN are always significantly higher than those for G/G/G. In general, a large internal friction coefficient can make the system work more steadily, so the results indicate that structural stability of the trilayer BN/G/BN should be higher than that of the G/G/G. To understand the differences between G/G/G and BN/G/BN, the deformation electron density and its isoline structure are further calculated and analyzed by DFT. Fig. 6 shows the deformation electron density and its section isoline by simulating G/G/G and BN/G/BN model with interlayer compression and midlayer sliding distances of 0.15 and o.4 Å, respectively. The electron density is the same as the online equivalent and it gradually becomes smaller on the vertical isolines from the inside outward. The isoline intervals reflect the local electronic conditions in that the greater the interval, the weaker is the localization and the more are the free electrons, and vice versa. As shown in Figs. 6(a1) and (b1), the outer-layer electrons for BNNSs are obviously partial to the N atom in the B–N bond. However, for graphenes, the electrons are more concentrated at the center of the C–C bond. The outer-layer electrons are the main cause of the covalent bond. If the outer-layer electrons spend most of their time within the nuclei of the two atoms, then the covalent bond is placed in the bonding orbital, in which case the distribution of the electron density is small at either end and large in the middle. In contrast, if the electrons spend most of their time outside the nuclei of the two atoms, then the covalent bond is placed in the antibonding orbital, in which case the distribution of

the electron density is large at both ends and small in the middle. This is because in the bonding orbital electron density between the nuclei increases whereas in the antibonding orbital it decreases. Placing an electron in the bonding orbital stabilizes the molecule because it remains in between the two nuclei. Conversely, placing electrons in the antibonding orbital causes a decrease in stability [53]. The deformation electron density plot in Fig. 6 shows that each layer of graphenes in G/G/G has a good bonding electronic distribution that is small at each end and large in the middle. The electrons are mainly uniformly distributed along the atoms in rings on the plane and there are fewer electrons in the out-plane (see Fig. 6(a2) ), resulting in weak interaction between up-down neighboring nanosheets for G/G/G. However, the situation for BN/G/BN is somewhat different. Because the different kinds of atoms exist between up-down nanosheets and the polar covalent bond exists in B–N bond, electronegativity becomes a dominant factor. The electronic localization of the inner layer may be weakened, some $s$ electrons become $p$ electrons due to excitation and partial electronic delocalization of the outer shell occurs, which results in an increase in electron mobility. Consequently, there are more electrons between up-down neighboring nanosheets (see Fig. 6(b2) ), showing a long range attraction between up-down neighboring nanosheets. Obviously, the resistance in BN/G/BN should be greater than that in G/G/G when mid-layer graphene is drawn out of trilayer nanosheets along its plane, naturally resulting in the higher internal friction coefficients in BN/G/BN. In the meantime, this also explains, more intuitively, that

the structural stability of the trilayer BN/G/BN is higher than that of the G/G/G from another angle.

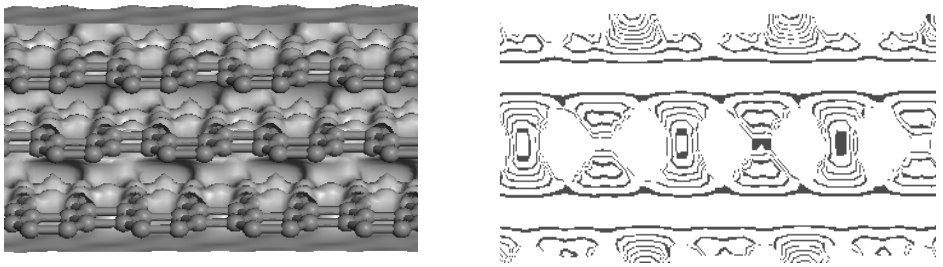

(a1) (a2)

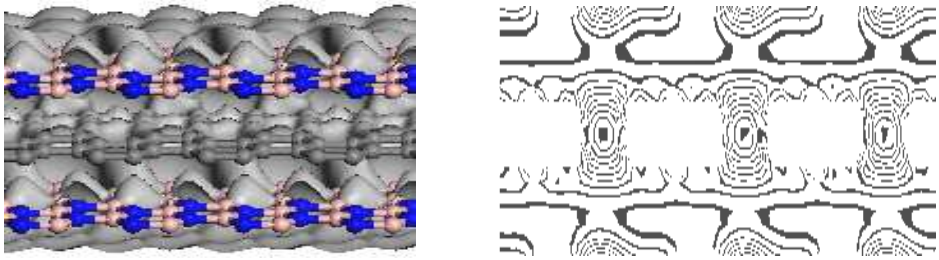

(b1) (b2)

Fig. 6. Deformation electron density (left) and isoline structure (right) on cross section of G/G/G (a1, a2) and BN/G/BN (b2, b2) with the compressed interlayer distances of 0.15 Å.

It can be further concluded through Fig. 5 that the coefficients for both G/G/G and BN/G/BN increase with the pressure. The growth rate can be divided into three stages. The pressure for relatively quick increases is in the less than 50nN range, that for slow increase is in the range of 50 to170nN and the saturation phenomenon on the variation of friction coefficients with pressure occurs in the greater than 170nN range, that is, the friction coefficients are basically constant, not varying with the

pressure, following the simple microscopic theory of Amontons's laws [54]. Because the friction coefficients of the graphenes are related to surface structure, roughness and environment, the experimental results are not a constant value - values are in a range of 0.006 to 0.45 [55-57]. The calculated results in this paper are obviously within the range of the experiment datum.

### 3.3 In-plane natural frequency of mid-layer graphenes in trilayer nanosheets

As seen in Fig. 4, with the normal pressure on trilayer nanosheets, a periodic potential obviously emerges along x direction. It is natural to create a restoring force nearby the minimum potential energy (equilibrium position). By fitting the curve around the equilibrium position, it can be found that the restoring force has a good linear correlation with displacement to equilibrium position. As we all know, graphene possesses an ultrahigh intrinsic strength and stiffness, so the mid-layer graphene in trilayer nanosheets can be approximately considered as a rigid whole. Therefore, if the thermal effect is neglected, the equation of free vibration on the mid-layer graphenes along x direction can be expressed as:

$$M\ddot{x} + kx = 0 \tag{9}$$

where $M$ and $k$ are total mass and equivalent elastic coefficient of sliding system, respectively, $\ddot{x}$ and $x$ are the acceleration and displacement to equilibrium position, respectively. The equivalent elastic coefficients $k$ can be obtained by the following formula:

$$k = \partial^2 U(x, F_N) / \partial x^2 \tag{10}$$

The second order polynomial is used to fit the computing data of potential energy to sliding displacement near the minimum potential energy in Fig. 4, and then the equivalent elastic coefficients $k$ under different lengths of compression are calculated (Fig. 7).

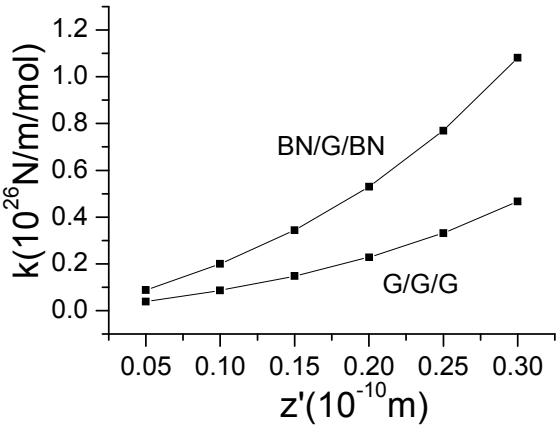


Fig. 7. The equivalent elastic coefficients $k$ as a function of different lengths of compression.

According to the general resonance theory, the natural frequency can be calculated as follows:

$$\nu = \frac{1}{2\pi}\sqrt{\frac{k}{M}} \tag{11}$$

Based on the formula, combined with the results in table 2, the natural frequency under different normal pressures can be obtained, as shown in Fig. 8.

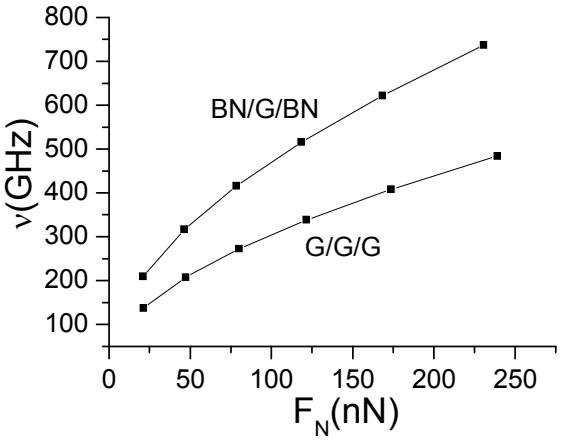


Fig. 8. The natural frequency as a function of different normal pressures.

It can be seen from Fig. 8 that the natural frequency of mid-layer graphene in its plane direction increases with the increase in normal pressure. The natural frequency in BN/G/BN is significantly higher than in G/G/G, and both of them increase with the pressure. Through data fitting, the function relation between the normal pressure and the natural frequency can be obtained as follows:

$$\nu = 93.54397 + 2.44859F_N - 0.00346F_N{}^2 \qquad \text{for G/G/G} \qquad (12)$$

$$\nu = 141.09183 + 3.83886F_N - 0.00552F_N{}^2 \qquad \text{for BN/G/BN} \qquad (13)$$

where $\nu$ is the natural frequency for the mid-layer graphene in its plane direction, GHz; $F_N$ is the external normal pressure, nN. Obviously, a change of external pressure for trilayer nanosheets can be perceived by the change of in-plane natural frequency for mid-layer grapheme through the function relation between the normal pressure and the natural frequency.

Equations (12) and (13) show that the change of natural frequency is of the order of GHz and the external normal pressure is of the order of nN and, therefore, the in-plane natural frequency for mid-layer graphene in trilayer nanosheets is extremely sensitive to external pressure loads, especially for mid-layer graphene in BN/G/BN. This feature implies a huge application foreground in micro/nano force sensor.

## 4. Conclusion

By calculating the interlaminar interaction of trilayer coupled structures under different external normal pressures and their potential energies at different relative sliding positions of the mid-layer graphene, the internal friction and natural frequency in trilayer nanosheets G/G/G and BN/G/BN are examined. The results indicate that the internal friction coefficients for G/G/G and BN/G/BN are about 0.015 and 0.025, respectively. The internal friction coefficients for BN/G/BN is significantly higher than that for G/G/G. The coefficients for both G/G/G and BN/G/BN increase with the increase of pressure at three growth rates. The pressure for relatively quick increase occurs in the less than 50nN range, that for slow increase is in the range of 50 to 170nN and the saturation phenomenon for the friction coefficients to the pressure occurs in the greater than 170nN range, that is, the friction coefficients vary little with the pressure change, following simple microscopic theory of Amontons's laws. These results are useful for understanding the mechanism of nano-tribology and provide an effective micro-control method of internal friction.

Further analysis indicates that the in-plane natural frequency of mid-layer graphene in trilayer complexes increases with the increase in external normal pressure and the natural frequency in BN/G/BN is significantly higher than in G/G/G. It is found that the in-plane natural frequency is extremely sensitive to external pressure loads, especially for mid-layer graphene in BN/G/BN. Compared with traditional materials, graphene in BN/G/BN may potentially be a new sensing element in micro/nano force sensors, which have promising applications prospects in future M/NEMS.

## Acknowledgements

The work described in this paper was supported by grants from the Research Grants Council of the Hong Kong Special Administrative Region, China (Project No. 9042047, CityU 11208914) and National Natural Science Foundation of China (Grant No. 51378448). The work was also supported by Hunan Provincial Natural Science Foundation of China (Project No. 14JJ2076), Scientific Research Fund of Hunan Provincial Education Department, China (Project No. 12A001), the Construct Program of the Key Discipline in Hunan Province and Aid Program for Science and the Technology Innovative Research Team in Higher Educational Institutions of Hunan Province, China.

## References


1. F. P. Bowden, *The friction and lubrication of solids. [1]*, Clarendon Press, 1958.
2. A. H. Castro Neto, F. Guinea, N. M. R. Peres, K. S. Novoselov and A. K. Geim, *Rev. Mod. Phys.*, 2009, 81, 109-162.
3. A. A. Balandin, S. Ghosh, W. Z. Bao, I. Calizo, D. Teweldebrhan, F. Miao and C. N. Lau, *Nano Letters*, 2008, 8, 902-907.
4. C. Lee, Q. Y. Li, W. Kalb, X. Z. Liu, H. Berger, R. W. Carpick and J. Hone, *Science*, 2010, 328, 76-80.
5. J. Li, Z. H. Zhang, G. Kwong, W. Tian, Z. Q. Fan and X. Q. Deng, *Carbon*, 2013, 61, 284-293.
6. A. K. Geim and K. S. Novoselov, *Nat. Mater.*, 2007, 6, 183-191.
7. A. K. Geim, *Science*, 2009, 324, 1530-1534.
8. Z. H. Zhang, X. Q. Deng, X. Q. Tan, M. Qiu and J. B. Pan, *Applied Physics Letters*, 2010, 97.
9. N. N. Klimov, S. Jung, S. Z. Zhu, T. Li, C. A. Wright, S. D. Solares, D. B. Newell, N. B. Zhitenev and J. A. Stroscio, *Science*, 2012, 336, 1557-1561.
10. G. Gudehus, *Mechanics of Cohesive-frictional Materials*, 1998, 3, 365-365.
11. G. Binning, H. Rohrer, C. Gerber and E. Weibel, *Physical Review Letters*, 1982, 49, 57-61.
12. G. Binnig, C. F. Quate and C. Gerber, *Physical Review Letters*, 1986, 56, 930-933.
13. C. M. Mate, G. M. McClelland, R. Erlandsson and S. Chiang, *Physical Review Letters*, 1987, 59, 1942-1945.
14. A. Smolyanitsky, S. Z. Zhu, Z. Deng, T. Li and R. J. Cannara, *RSC Adv.*, 2014, 4, 26721-26728.
15. Z. Deng, A. Smolyanitsky, Q. Y. Li, X. Q. Feng and R. J. Cannara, *Nat. Mater.*, 2012, 11, 1032-1037.
16. M. Weiss and F. J. Elmer, *Physical Review B*, 1996, 53, 7539-7549.
17. W. Zhong and D. Tomanek, *Physical Review Letters*, 1990, 64, 3054-3057.
18. D. Tomanek, W. Zhong and H. Thomas, *Europhysics Letters*, 1991, 15, 887-892.
19. K. Matsushita, H. Matsukawa and N. Sasaki, *Solid State Commun.*, 2005, 136, 51-55.
20. H. Zaidi, D. Paulmier, A. Jeanmaire and H. Nery, *Surf. Sci.*, 1991, 251, 778-781.
21. R. Neitola, H. Ruuska and T. A. Pakkanen, *J. Phys. Chem. B*, 2005, 109, 10348-10354.
22. T. Filleter, J. L. McChesney, A. Bostwick, E. Rotenberg, K. V. Emtsev, T. Seyller, K. Horn and R. Bennewitz, *Physical Review Letters*, 2009, 102.
23. T. Filleter and R. Bennewitz, *Physical Review B*, 2010, 81.
24. C. Lee, X. D. Wei, Q. Y. Li, R. Carpick, J. W. Kysar and J. Hone, *Phys. Status Solidi B-Basic Solid State Phys.*, 2009, 246, 2562-2567.
25. Z. Deng, N. N. Klimov, S. D. Solares, T. Li, H. Xu and R. J. Cannara, *Langmuir*, 2013, 29, 235-243.
26. T. Murmu and S. C. Pradhan, *Journal of Applied Physics*, 2009, 105.
27. S. C. Pradhan and J. K. Phadikar, *Physics Letters A*, 2009, 373, 1062-1069.
28. T. Murmu and S. C. Pradhan, *Physica E*, 2009, 41, 1628-1633.
29. J. S. Bunch, A. M. van der Zande, S. S. Verbridge, I. W. Frank, D. M. Tanenbaum, J. M. Parpia, H. G. Craighead and P. L. McEuen, *Science*, 2007, 315, 490-493.

30. D. Garcia-Sanchez, A. M. van der Zande, A. S. Paulo, B. Lassagne, P. L. McEuen and A. Bachtold, *Nano Letters*, 2008, 8, 1399-1403.
31. R. A. Barton, B. Ilic, A. M. van der Zande, W. S. Whitney, P. L. McEuen, J. M. Parpia and H. G. Craighead, *Nano Letters*, 2011, 11, 1232-1236.
32. A. Eichler, J. Moser, J. Chaste, M. Zdrojek, I. Wilson-Rae and A. Bachtold, *Nature Nanotechnology*, 2011, 6, 339-342.
33. J. W. Jiang, J. S. Wang and B. W. Li, *Physical Review B*, 2009, 80.
34. O. Hod and G. E. Scuseria, *Nano Letters*, 2009, 9, 2619-2622.
35. K. Eom, H. S. Park, D. S. Yoon and T. Kwon, *Phys. Rep.-Rev. Sec. Phys. Lett.*, 2011, 503, 115-163.
36. M. Poot and H. S. J. van der Zant, *Phys. Rep.-Rev. Sec. Phys. Lett.*, 2012, 511, 273-335.
37. A. M. van der Zande, R. A. Barton, J. S. Alden, C. S. Ruiz-Vargas, W. S. Whitney, P. H. Q. Pham, J. Park, J. M. Parpia, H. G. Craighead and P. L. McEuen, *Nano Letters*, 2010, 10, 4869-4873.
38. F. Scarpa, S. Adhikari and R. Chowdhury, *Physics Letters A*, 2010, 374, 2053-2057.
39. Y. M. Shi, C. Hamsen, X. T. Jia, K. K. Kim, A. Reina, M. Hofmann, A. L. Hsu, K. Zhang, H. N. Li, Z. Y. Juang, M. S. Dresselhaus, L. J. Li and J. Kong, *Nano Letters*, 2010, 10, 4134-4139.
40. Z. H. Zhang, C. Guo, D. J. Kwong, J. Li, X. Q. Deng and Z. Q. Fan, *Advanced Functional Materials*, 2013, 23, 2765-2774.
41. W. Bao, L. Jing, J. Velasco, Y. Lee, G. Liu, D. Tran, B. Standley, M. Aykol, S. B. Cronin, D. Smirnov, M. Koshino, E. McCann, M. Bockrath and C. N. Lau, *Nature Physics*, 2011, 7, 948-952.
42. F. Zhang, B. Sahu, H. K. Min and A. H. MacDonald, *Physical Review B*, 2010, 82, 035409.
43. R. G. Quhe, J. X. Zheng, G. F. Luo, Q. H. Liu, R. Qin, J. Zhou, D. P. Yu, S. Nagase, W. N. Mei, Z. X. Gao and J. Lu, *Npg Asia Materials*, 2012, 4, E6.
44. J. Slawinska, I. Zasada, P. Kosinski and Z. Klusek, *Physical Review B*, 2010, 82, 085431.
45. J. H. Yuan, J. X. Liao, C. H. Yang and X. H. Shi, *Current Nanoscience*, 2013, 9, 324-329.
46. J. H. Yuan and K. M. Liew, *Journal of Nanoscience and Nanotechnology*, 2012, 12, 2617-2624.
47. J. H. Yuan and K. M. Liew, *Carbon*, 2011, 49, 677-683.
48. K. M. Liew and J. H. Yuan, *Nanotechnology*, 2011, 22, 085701.
49. J. H. Yuan and K. M. Liew, *Journal of Physical Chemistry C*, 2011, 115, 431-435.
50. A. K. Rappe, C. J. Casewit, K. S. Colwell, W. A. Goddard and W. M. Skiff, *Journal of the American Chemical Society*, 1992, 114, 10024-10035.
51. C. J. Casewit, K. S. Colwell and A. K. Rappe, *Journal of the American Chemical Society*, 1992, 114, 10035-10046.
52. L. Boldrin, F. Scarpa, R. Chowdhury and S. Adhikari, *Nanotechnology*, 2011, 22, 505702.
53. D. W. Smith, *J. Chem. Educ.*, 2000, 77, 780-784.
54. M. H. Muser, L. Wenning and M. O. Robbins, *Physical Review Letters*, 2001, 86, 1295-1298.
55. J. A. Ruan and B. Bhushan, *Journal of Applied Physics*, 1994, 76, 8117-8120.
56. J. Sugishita and S. Fujiyoshi, *Wear*, 1981, 68, 7-20.
57. H. Zaidi, E. Csapo, H. Nery, D. Paulmier and T. Mathia, *Surf. Coat. Technol.*, 1993, 62,

388-392.

**A list of captions for figures and tables:**

Fig. 1. Geometric models of trilayer BN/G/BN and G/G/G (unit: nm).

Fig. 2. The interaction energies as a function of length of compression in G/G/G and BN/G/BN.

Fig. 3. The normal pressures as a function of length of compression in G/G/G and BN/G/BN.

Fig. 4. The potential energies as a function of the sliding distances under different normal pressures in G/G/G and BN/G/BN. (A) Periodogram $z'$=0.05 Å (B) Calculation diagrams (a) $z'$=0.05 Å (b) $z'$=0.10 Å (c) $z'$=0.15 Å (d) $z'$=0.20 Å (e) $z'$=0.25 Å (f) $z'$=0.30 Å

Fig. 5. The frictional coefficients as a function of different pressures.

Fig. 6. Deformation electron density (left) and isoline structure (right) on cross section of G/G/G (a1, a2) and BN/G/BN (b2, b2) with the compressed interlayer distances of 0.15 Å.

Fig. 7. The equivalent elastic coefficients $k$ as a function of different lengths of compression.

Fig. 8. The natural frequency as a function of different normal pressures.

Table 1. Single-point energies of graphene and BNNS in BN/G/BN and G/G/G ($10^6$ J/mol)

Table 2. The normal pressures at different lengths of compression (nN).